Enhanced respiratory electron dissipation promotes mycobacterial biofilm longevity

Kaushik Poddar[1], Snehal V. Khairnar[1], Amitesh Anand[1,*]

[1]Department of Biological Sciences, Tata Institute of Fundamental Research, Mumbai, Maharashtra 400005, India.
*amitesh.anand@tifr.res.in

Abstract

Mycobacterium tuberculosis organizes as multicellular structures like granuloma and biofilm within human lungs and these lifestyles are critical for the pathophysiological outcomes. Granuloma has been the hallmark of *M. tuberculosis* infection and has been studied extensively. However, the biofilm development and survival remains poorly understood. We show that supplementation of immunometabolites, nitrate or fumarate, extends mycobacterial biofilm lifespan dramatically. This longevity is enabled by suppression of dormancy regulons and maintenance of active metabolic state under nitrate. These results establish that access to alternative electron acceptors directly influences mycobacterial biofilm fate. By linking dormancy suppression to prolonged structural integrity, our study identifies respiratory flexibility as a determinant of mycobacterial biofilm persistence. These findings reveal a central metabolic lever that dictates biofilm survival and open new avenues for targeting mycobacterial biofilms in clinical settings.

Introduction

Mycobacterium tuberculosis, the etiological agent of tuberculosis (TB), persists within host-derived multicellular structures known as granulomas [1]. In addition to these host-mediated assemblies, mycobacteria can generate self-produced multicellular formations, including cords and biofilms [2,3]. These diverse structural lifestyles are intricately linked to TB pathophysiology. While granuloma formation remains a defining hallmark of TB, cord formation represents a pivotal event in early pathogenesis, and biofilm development during infection has been shown to enhance mycobacterial virulence [2,4,5]. Notably, such multicellular structures exhibit elevated drug tolerance and are implicated in the emergence of antibiotic resistance.

Biofilms are a widespread mode of bacterial community organization that follow an aging cycle [6]. Their development begins when cells attach to a suitable surface and proliferate to form a mature structure, in which they become embedded within an extracellular matrix. As biofilms mature, they acquire a multilayered architecture, with bacterial populations adopting metabolic states tailored to the local physico-chemical environment. Despite mounting evidence for the clinical importance of the mycobacterial biofilm lifestyle, its mechanisms of development and dispersal remain poorly understood.

The metabolic interplay between the host and microbes play a crucial role in influencing colonization outcomes. Pathogens can exploit and manipulate host microenvironments to enhance their survival [7]. During infection, host-derived nitric oxide is converted to nitrate under conditions of high oxidative stress within the inflamed niche. Nitrate has been shown to promote mycobacterial growth in macrophages [8,9]. Similarly, host derived short-chain fatty acids also modulate mycobacterial metabolism and colonisation success [10,11]. Despite these insights, the effect of such host metabolites on the physiology of mycobacterial biofilms—structures that confer persistence and drug tolerance—remains poorly understood. Defining this relationship is therefore critical to elucidating metabolic adaptations that underlie biofilm-associated tuberculosis.

We examined a panel of immunometabolites for their influence on mycobacterial biofilm survival. In this study, we demonstrate that metabolites reinforcing respiratory electron dissipation fundamentally reshapes biofilm physiology by—(a) nearly doubling biofilm lifespan, (b) suppressing the dormancy regulon to extend longevity, and (c) sustaining metabolic activity to overcome energetic constraints.

Results and discussion

Modulation of mycobacterial biofilm by immunometabolites

We used an in vitro model of *M. smegmatis* biofilm to examine the impact of several immunometabolites. In Sauton's medium, *M. smegmatis* establishes a robust biofilm at the air–liquid interface, reaching maturity within five days. Beyond this point, the pellicle gradually loses structural integrity and ultimately sinks to the bottom of the well, a transition that likely reflects the biofilm dispersal (Figure 1A) [12].

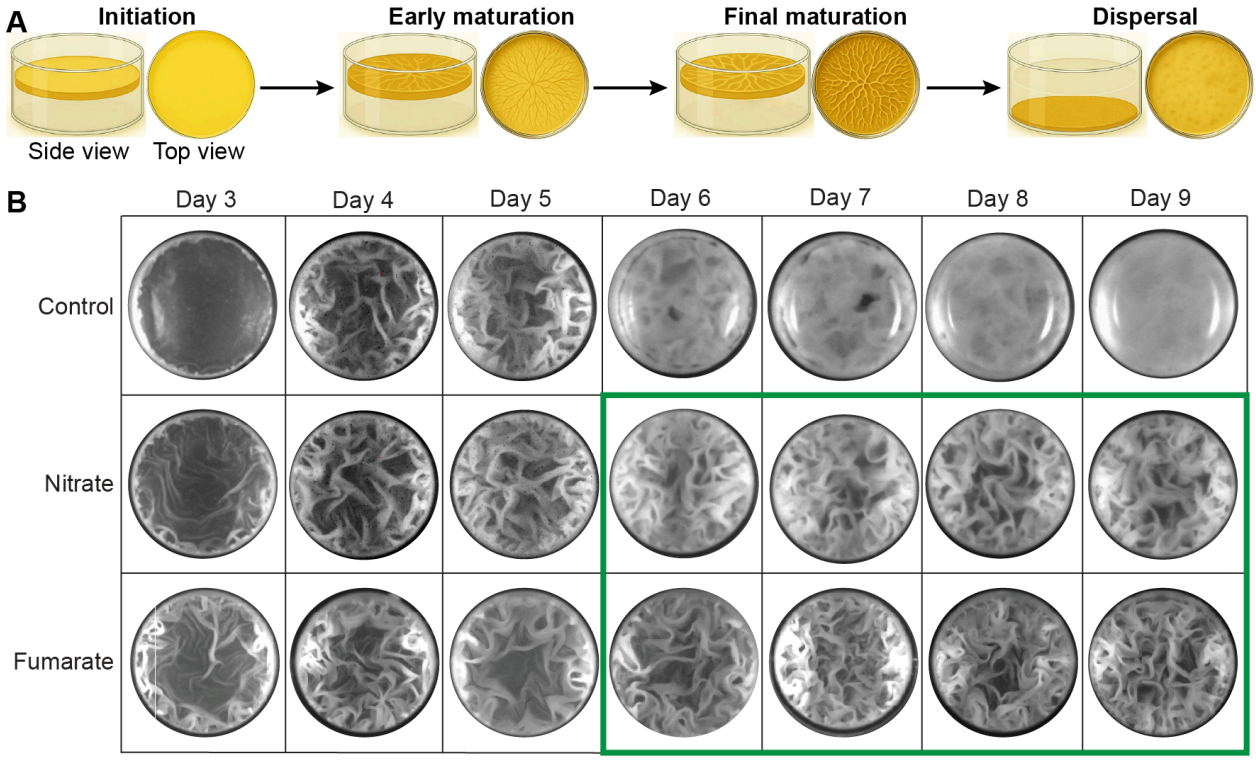

Figure 1: Influence of nitrate and fumarate on the life-span of mycobacterial biofilm. (A) A schematic generated using ChatGPT (OpenAI) showing various stages of in vitro mycobacterial biofilm. (B) Effect of sodium nitrate and sodium fumarate supplementation on *M. smegmatis* biofilm morphology (top view). Columns are for the age of the biofilm in days and rows are for metabolites that are supplemented (1% weight/volume) in the biofilm culture.

We inoculated *M. smegmatis* in biofilm forming media with the following supplements: (a) short-chain fatty acids (acetate, pyruvate, formate), (b) fumarate and (c) nitrate. We observed that, while formate did not show any appreciable impact, supplementation of acetate, pyruvate, fumarate and nitrate hastened the biofilm development (Supp. Figure 1). Interestingly, fumarate and nitrate showed remarkable influence on biofilm lifespan. The untreated biofilms typically disperse by day six, whereas nitrate or fumarate supplementation prolonged biofilm integrity beyond nine days (Figure 1B). The longevity influence was specific to biofilm as we did not observe any significant effect on planktonic cultures (Supp. Figure 2). Mature biofilms can restrict oxygen diffusion across their layers, leading to pronounced hypoxia in the core population [13,14]. Both fumarate and nitrate can function as alternate electron acceptors and facilitate electron dissipation. Notably, *M. smegmatis* possesses the metabolic abilities to use nitrate and fumarate as terminal electron acceptors in its respiratory electron transport system [15] .

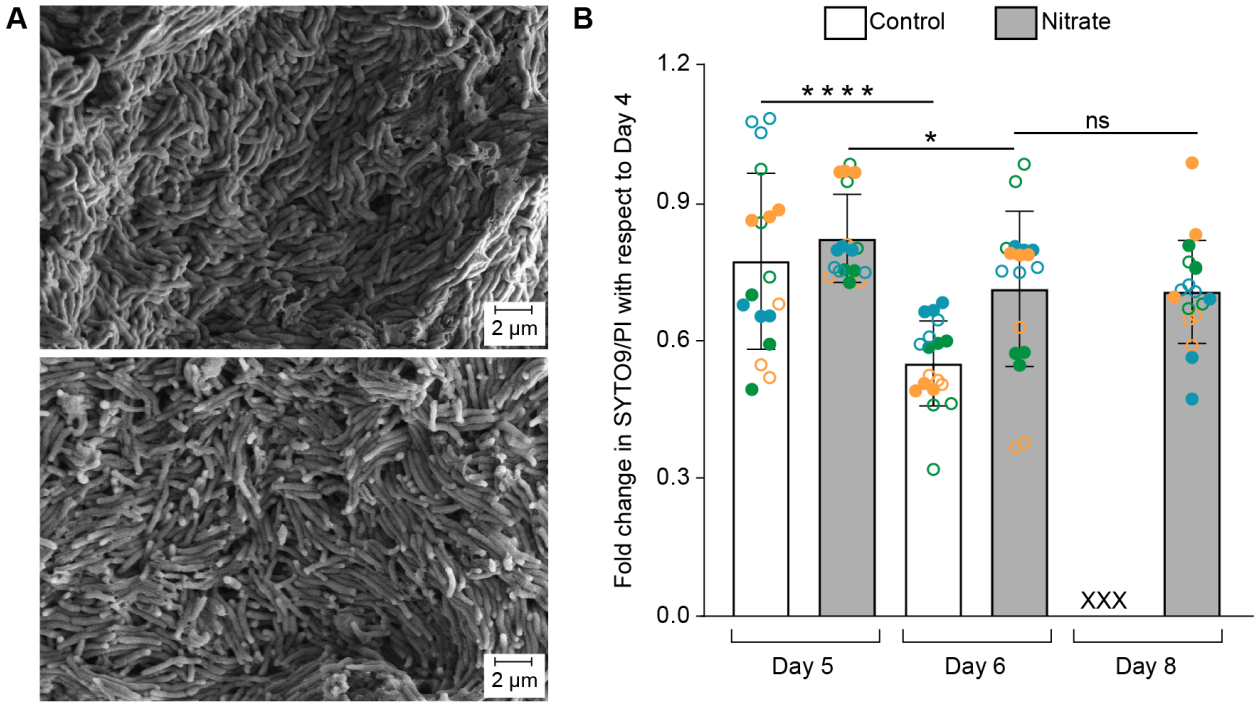

Figure 2: Influence of nitrate on the cells within mycobacterial biofilm. (A) Scanning electron micrograph of *M. smegmatis* biofilms at 10kX magnification (control on the top and 1% sodium nitrate supplemented on the bottom). (B) Fold change in ratio of fluorescence readings of SYTO green-fluorescent nucleic acid stain (SYTO9) and propidium iodide (PI). The unsupplemented biofilm disperses by day 6, so there is no experimental value for day 8. Circles differing either in color or pattern represent different biological replicates. Error bars are showing standard deviation and Unpaired t-test has been used for statistical analysis (ns: non significant, *: p-value < 0.05 and ****: p-value < 0.0001).

The pronounced extension in biofilm lifespan prompted us to examine whether these metabolites influenced biofilm architecture or cellular survival. We performed further analyses using nitrate which is an established terminal electron acceptor for mycobacteria. Although scanning electron micrographs revealed no major alteration in cellular organization, nitrate-treated biofilms exhibited markedly improved cell viability (Figure 2A, 2B). The mitigation of the decline in live-to-dead cell ratio upon nitrate supplementation suggests that nitrate respiration enhances redox balance and supports hypoxic survival within the biofilm.

Transcriptional rewiring governing mycobacterial biofilm aging

To investigate the mechanistic link between nitrate supplementation and biofilm aging, we performed temporal profiling of the transcriptome. We observed a clear segregation of age-associated transcriptomes along the first principal component (Figure 3A). Interestingly the transcriptome of nitrate-supplemented biofilm localized closer to the samples from an earlier

day. We performed a single-sample gene set enrichment analysis to evaluate pathway activity across samples [16]. Transcriptomic profiles segregated into five clusters based on the expression of pathway-associated genes (Supp. Figure 3). As expected, cluster 3—the largest cluster, enriched for nitrogen metabolism—showed elevated activity in nitrate-supplemented samples. Interestingly, in the second-largest cluster (cluster 2), the Z-scores of day 5 nitrate-supplemented samples closely resembled those of day 4 controls, indicating a nitrate-mediated delay in biofilm aging.

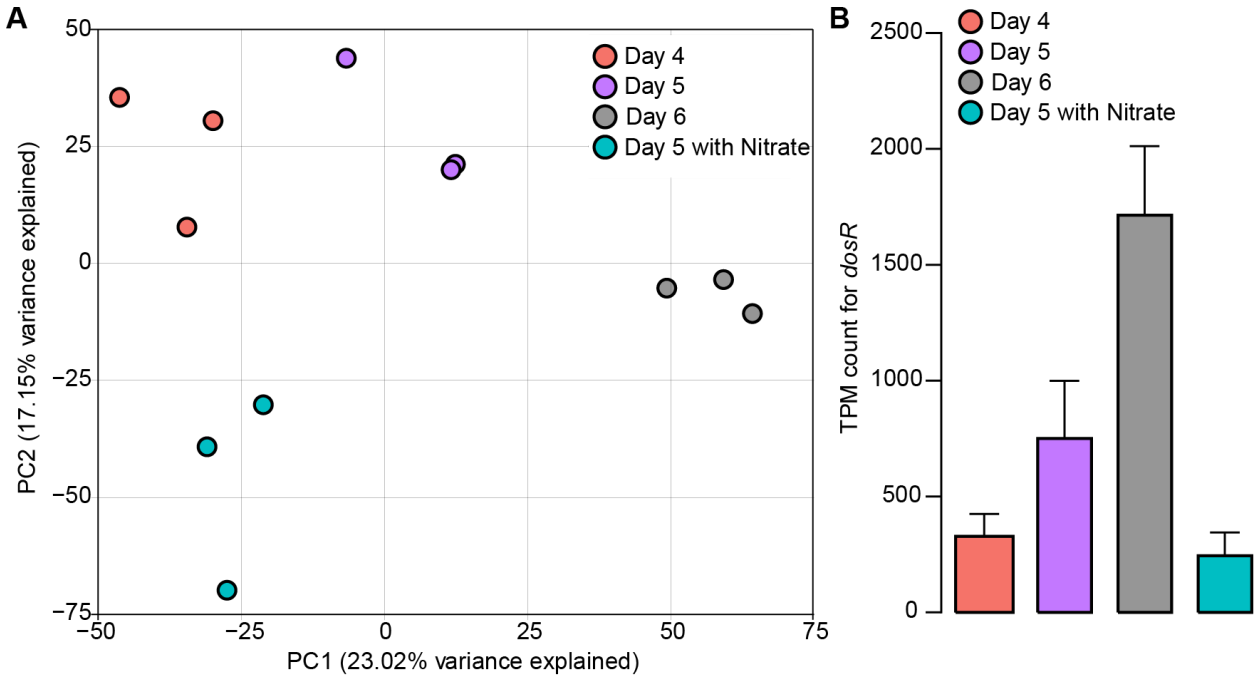

Figure 3: Nitrate induced transcriptional rewiring to prolong *M. smegmatis* biofilm life-span. (A) Transcriptome based distribution of biofilm samples along first and second principal component axes. (B) Temporal expression profile of the dormancy regulator *dosR* in the biofilm (error bar represents standard deviation).

Mycobacterial cells tend to enter a dormant state to survive low oxygen conditions [17]. The biofilm of *M. tuberculosis* shows decreased expression of dormancy regulon (DosR regulon) [18]. However, a temporal transcriptomic profiling of aging *M. bovis* BCG biofilm showed progressive increase in the expression of *dosR* [19]. We observed a transcriptional upregulation in the DosR regulon in *M. smegmatis* biofilm (Figure 3B and Supp. Figure 4). Remarkably, nitrate supplementation suppressed the activation of dormancy in maturing biofilm, thereby, extending the lifespan by providing a conducive metabolic state.

The rewiring in carbon metabolism and respiratory pathways allows environment-specific tailoring of cellular physiology. *M. tuberculosis* shifts to a non-replicating persistent (NRP) state when ambient oxygen concentration decreases gradually [20]. This drug tolerant state is a hallmark of TB granuloma and results from a decrease in metabolic activities [21]. The metabolic gene expression pattern of hypoxic NRP cells showed a remarkable overlap with dispersing biofilm cells, with a shift to fermentative energetics (Figure 4A) [22]. Similarly, there was a temporal increase in the expression of high affinity dioxygen reductase- cytochrome bd oxidase- potentially in an attempt to maintain some respiratory activity under oxygen deprivation (Figure 4B). The reinforcement of electron dissipation through nitrate resulted in lesser reliance on cytochrome bd oxidase and the expression went down to levels as in oxygen -sufficient early biofilm stage.

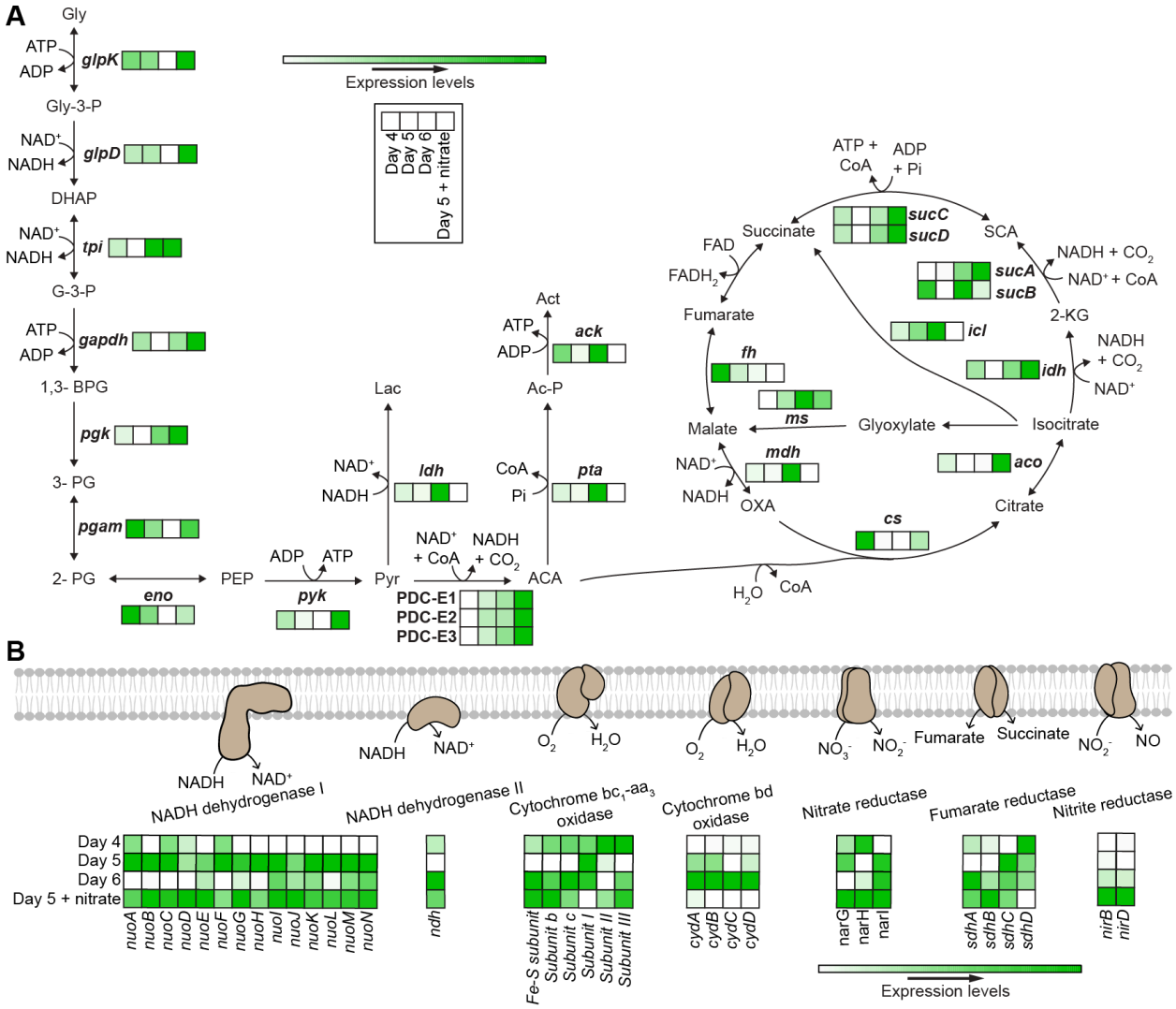

Figure 4: Nitrate induced transcriptional rewiring in metabolic pathways to prolong *M. smegmatis* biofilm life-span. Expression profile of the genes involved in the (A) central carbon metabolism reactions and (B) electron transport system. The expression profile is an average of TPM (transcript per million) counts from three biological replicates. The detailed TPM counts are reported in Supp. Sheet 1.

Concluding remarks

Our data suggest impaired electron dissipation as a factor causing dispersal of mycobacterial biofilm and mitigating this stress promotes lifespan extension. Given that pathogens encounter a dynamic host milieu enriched with diverse metabolites, shifts in chemical balance—such as the elevated nitrate-to-nitrite ratio favoring *Pseudomonas aeruginosa* colonization in bronchiectasis—underscore the importance of host-derived cues in shaping infection [23]. *M. tuberculosis* also colonizes lung tissues and forms biofilms, dissecting how microenvironmental components govern its growth and persistence is critical. Notably, modulation of non-replicating persistence signatures may not only alter disease trajectory but also influence therapeutic efficacy.

Materials and methods

Mycobacterium smegmatis mc^2155 (ATCC- 700084) was used in this study. All reagents used, except SYTO green fluorescent nucleic acid stain (Invitrogen), propidium iodide (Invitrogen) and TRIzol (Invitrogen), were from Sigma.

Planktonic and biofilm growth profiling

Tecan Spark multimode microplate reader was used for growth profiling. Log phase culture of *M. smegmatis* was used to set up growth characterization experiments in 96-well plates. The initial OD600 was set to 0.05 in Sauton's media containing 0.05% Tween 80. Growth curves were set in three technical replicates each. The cultures were incubated at 37℃ in shaking condition. Sodium nitrate and sodium fumarate were supplemented to the media as required. Biofilms were set-up using protocol as described previously [12] in 24-well plates with 1.5 mL media. Sodium nitrate, sodium fumarate, sodium acetate, sodium pyruvate and sodium formate were supplemented to the media as required.

Scanning electron microscopy

5 day old biofilms were used for scanning electron microscopy. The media from the wells were removed carefully. After washing once with 1X PBS, 2.5% glutaraldehyde (made in 1X PBS) was added and incubated overnight at 4℃ in the dark for fixation. Glutaraldehyde was then removed and again washed with 1x PBS. Samples were then treated with 1% OsO_4 for 1 hour. After removing the OsO_4, samples were washed again with 1X PBS. Finally dehydration of the samples were done by sequential washing with 50%, 70%, 80%, 90% and 100% ethanol. Finally after drying, samples were loaded onto stubs and gold coated for 1 minute at 10mA and imaged using Zeiss Ultra 55 plus.

SYTO9/PI assay

Biofilm cells from control and 1 % nitrate treated conditions were harvested from one well and washed with 1X PBS. 5 uM SYTO9 and PI (made in 1X PBS) were added to the cells and incubated in the dark for 20 minutes. Cells were again washed with 1X PBS to remove any unbound dye. 200 uL of the samples were added to three wells for each sample in black colored, clear bottom 96-well plates. The fluorescence intensity was measured using Tecan Spark multimode microplate reader. For SYTO9, the excitation and emission wavelengths were 405 nm and 525 nm respectively. For PI, the excitation and emission wavelengths were 561 nm and 625 nm respectively.

RNAsequencing

RNA was extracted from 4, 5 and 6 days old biofilms with or without 1% sodium nitrate using Qiagen miRNeasy Mini kit (Cat. No. 1038703). Biofilm cells were homogenized and lysed in TRIzol reagent by bead-beating and RNA isolation was performed following the manufacturer suggested protocol. 250 ng of RNA sample was used for ribodepletion by using NEBNext rRNA depletion kit Bacteria (Cat. no. NEB E7850X), according to the manufacturer's protocol. The NEBNext Ultra II Directional RNA Library prep kit for Illumina (Cat. no. E7760L), was used to construct double-stranded cDNA libraries and sequenced using Illumina NextSeq 2000.

RNA-seq data were processed as described in [24], except that reads were mapped to the *M. smegmatis* (NC_008596) reference genome. The batch correction of RNA-seq count data was done using ComBat-seq [25]. Principal component analysis (PCA) was conducted on batch corrected count data. PCA was implemented using the prcomp function in R on the transposed

expression matrix. The counts were variance-stabilized using the rlog transformation from DESeq2 [26].

Pathway activity analysis by ssGSEA

Single-sample gene set enrichment analysis was used to quantify pathway activity in individual transcriptomic samples [16]. The analysis was implemented using the GSEApy Python package [27] on TPM-normalized, batch-corrected expression data, with gene sets curated from KEGG pathways relevant to *M. smegmatis* [28]. For each experimental condition (Day 4, Day 5, Day 6, and Day 5 with nitrate supplementation), enrichment scores were standardized using Z-score normalization to facilitate direct comparison across conditions. The mean Z-scores of the three biological replicates, with error represented as the standard error of the mean, were then used to perform hierarchical clustering of pathways based on their temporal changes.This analysis yielded five distinct clusters: Cluster 1 (379 genes), Cluster 2 (458 genes), Cluster 3 (654 genes), Cluster 4 (63 genes), and Cluster 5 (236 genes).

Acknowledgments

This work was supported by the Ramalingaswami Re-entry Fellowship of the Department of Biotechnology, Government of India (BT/RLF/Re-entry/70/2020) and Tata Institute of Fundamental Research, Department of Atomic Energy, Government of India (19P0120) to Amitesh Anand. We acknowledge the support of the electron microscopy facility of TIFR, Mumbai, India. We thank Ms. Stuti Srivastav for her critical feedback on the manuscript.

Author contributions

Conceptualization and Supervision: A.A.; Experimentation: K.P.; Analysis: K.P., S.K., and A.A.; Manuscript writing: A.A. and K.P.

Data availability

RNAseq data supporting this study are deposited at GEO (GSE305991).

References:

1. Co, D.O., Hogan, L.H., Kim, S.-I., and Sandor, M. (2004). Mycobacterial granulomas: keys to a long-lasting host-pathogen relationship. Clin Immunol *113*, 130–136.

2. Mishra, R., Hannebelle, M., Patil, V.P., Dubois, A., Garcia-Mouton, C., Kirsch, G.M., Jan, M., Sharma, K., Guex, N., Sordet-Dessimoz, J., et al. (2023). Mechanopathology of biofilm-like Mycobacterium tuberculosis cords. Cell *186*, 5135–5150.e28.

3. Ojha, A.K., Baughn, A.D., Sambandan, D., Hsu, T., Trivelli, X., Guerardel, Y., Alahari, A., Kremer, L., Jacobs, W.R., Jr, and Hatfull, G.F. (2008). Growth of Mycobacterium tuberculosis biofilms containing free mycolic acids and harbouring drug-tolerant bacteria. Mol Microbiol *69*, 164–174.

4. Chakraborty, P., Bajeli, S., Kaushal, D., Radotra, B.D., and Kumar, A. (2021). Biofilm formation in the lung contributes to virulence and drug tolerance of Mycobacterium tuberculosis. Nat Commun *12*, 1606.

5. Barclay, A.M., Ninaber, D.K., Limpens, R.W.A.L., Walburg, K.V., Bárcena, M., Hiemstra, P.S., Ottenhoff, T.H.M., van der Does, A.M., and Joosten, S.A. (2024). Mycobacteria develop biofilms on airway epithelial cells and promote mucosal barrier disruption. iScience *27*, 111063.

6. Rumbaugh, K.P., and Sauer, K. (2020). Biofilm dispersion. Nat Rev Microbiol *18*, 571–586.

7. Srivastav, S., Biswas, A., and Anand, A. (2025). Interplay of niche and respiratory network in shaping bacterial colonization. J Biol Chem *301*, 108052.

8. Sohaskey, C.D. (2008). Nitrate enhances the survival of Mycobacterium tuberculosis during inhibition of respiration. J Bacteriol *190*, 2981–2986.

9. Cunningham-Bussel, A., Zhang, T., and Nathan, C.F. (2013). Nitrite produced by Mycobacterium tuberculosis in human macrophages in physiologic oxygen impacts bacterial ATP consumption and gene expression. Proc Natl Acad Sci U S A *110*, E4256–E4265.

10. Eoh, H., and Rhee, K.Y. (2013). Multifunctional essentiality of succinate metabolism in adaptation to hypoxia in Mycobacterium tuberculosis. Proc Natl Acad Sci U S A *110*, 6554–6559.

11. Silva, C.A. de M.E., Rojony, R., Bermudez, L.E., and Danelishvili, L. (2020). Short-Chain Fatty Acids Promote subsp. Growth in Nutrient-Limited Environments and Influence Susceptibility to Antibiotics. Pathogens *9*. https://doi.org/10.3390/pathogens9090700.

12. Poddar, K., and Anand, A. (2024). Growing Mycobacterial Biofilm as a Model to Study Antimicrobial Resistance. J Vis Exp. https://doi.org/10.3791/66607.

13. Anand, A., Verma, P., Singh, A.K., Kaushik, S., Pandey, R., Shi, C., Kaur, H., Chawla, M.,

Elechalawar, C.K., Kumar, D., et al. (2015). Polyketide Quinones Are Alternate Intermediate Electron Carriers during Mycobacterial Respiration in Oxygen-Deficient Niches. Mol Cell *60*, 637–650.

14. Patel, T.D., and Bott, T.R. (1991). Oxygen diffusion through a developing biofilm of pseudomonas fluorescens. J. Chem. Technol. Biotechnol. *52*, 187–199.

15. Khan, A., and Sarkar, D. (2012). Nitrate reduction pathways in mycobacteria and their implications during latency. Microbiology (Reading) *158*, 301–307.

16. Barbie, D.A., Tamayo, P., Boehm, J.S., Kim, S.Y., Moody, S.E., Dunn, I.F., Schinzel, A.C., Sandy, P., Meylan, E., Scholl, C., et al. (2009). Systematic RNA interference reveals that oncogenic KRAS-driven cancers require TBK1. Nature *462*, 108–112.

17. Rustad, T.R., Sherrid, A.M., Minch, K.J., and Sherman, D.R. (2009). Hypoxia: a window into Mycobacterium tuberculosis latency. Cell Microbiol *11*, 1151–1159.

18. Youngblom, M.A., Smith, T.M., Murray, H.J., and Pepperell, C.S. (2024). Adaptation of the Mycobacterium tuberculosis transcriptome to biofilm growth. PLoS Pathog *20*, e1012124.

19. Cruz-Villegas, M.A.D. la, Ares, M.A., Rodríguez-Valverde, D., Vallejo-Cardona, A.A., Flores-Valdez, M.A., Cota-Núñez, I.D., Aceves-Sánchez, M. de J., Lira-Chávez, J., Rodríguez-Campos, J., and Bravo-Madrigal, J. (2020). Transcriptional and Mycolic Acid Profiling in BCG In Vitro Show an Effect for c-di-GMP and Overlap between Dormancy and Biofilms. J Microbiol Biotechnol *30*, 811–821.

20. Bacon, J., Alderwick, L.J., Allnutt, J.A., Gabasova, E., Watson, R., Hatch, K.A., Clark, S.O., Jeeves, R.E., Marriott, A., Rayner, E., et al. (2014). Non-replicating Mycobacterium tuberculosis elicits a reduced infectivity profile with corresponding modifications to the cell wall and extracellular matrix. PLoS One *9*, e87329.

21. Lim, J., Lee, J.J., Lee, S.-K., Kim, S., Eum, S.-Y., and Eoh, H. (2021). Phosphoenolpyruvate depletion mediates both growth arrest and drug tolerance of in hypoxia. Proc Natl Acad Sci U S A *118*. https://doi.org/10.1073/pnas.2105800118.

22. Berney, M., and Cook, G.M. (2010). Unique flexibility in energy metabolism allows mycobacteria to combat starvation and hypoxia. PLoS One *5*, e8614.

23. Zhou, Y., He, X., Tang, J., Zhang, D., Liu, Y., Xue, Y. ’e, Jiang, N., Zhang, J., and Wang, X. (2024). Total sputum nitrate/nitrite is associated with exacerbations and colonisation in bronchiectasis. ERJ Open Res *10*. https://doi.org/10.1183/23120541.01045-2023.

24. Anand, A., Olson, C.A., Yang, L., Sastry, A.V., Catoiu, E., Choudhary, K.S., Phaneuf, P.V., Sandberg, T.E., Xu, S., Hefner, Y., et al. (2019). Pseudogene repair driven by selection pressure applied in experimental evolution. Nat Microbiol *4*, 386–389.

25. Zhang, Y., Parmigiani, G., and Johnson, W.E. (2020). ComBat-seq: batch effect adjustment for RNA-seq count data. NAR Genom Bioinform *2*, lqaa078.

26. Love, M.I., Huber, W., and Anders, S. (2014). Moderated estimation of fold change and dispersion for RNA-seq data with DESeq2. Genome Biol *15*, 550.

27. Fang, Z., Liu, X., and Peltz, G. (2023). GSEApy: a comprehensive package for performing gene set enrichment analysis in Python. Bioinformatics *39*. https://doi.org/10.1093/bioinformatics/btac757.

28. Kanehisa, M., Furumichi, M., Sato, Y., Matsuura, Y., and Ishiguro-Watanabe, M. (2025). KEGG: biological systems database as a model of the real world. Nucleic Acids Res *53*, D672–D677.